

1 **The changing character of twenty-first century precipitation over the**
2 **western United States in the variable-resolution CESM**

3 Xingying Huang, * Paul A. Ullrich

4 *Department of Land, Air and Water Resources, University of California, Davis*

5 *Corresponding author address: Xingying Huang, Department of Land, Air and Water Resources,
6 University of California Davis, Davis, CA 95616.
7 E-mail: xyhuang@ucdavis.edu

ABSTRACT

8 (To be added once the main content settled down)

9 **1. Introduction**

10 There is substantial and growing interest in the character of precipitation within a changing
11 climate, in large part because of the pronounced impacts of water availability on socioeconomic
12 and natural systems (Hegerl et al. 2004; Kharin et al. 2007; Scoccimarro et al. 2013). Among these
13 studies, precipitation extremes have been a major focus, particularly drought and flood events
14 (Seneviratne et al. 2012). Overall, it is widely agreed that although atmospheric water vapor
15 concentration is increasing, the impacts of a changing climate on the character of precipitation is
16 far more complicated. Extreme precipitation events are particularly nuanced: Our best projections
17 suggest that extreme precipitation events will intensify even in regions where mean precipitation
18 decreases (Tebaldi et al. 2006; Kharin et al. 2007).

19 Although future climate projections are subject to large uncertainties, climate models are essen-
20 tial tools for studying climate variability and extremes events in the future (Easterling et al. 2000).
21 Global climate models (GCMs) have often been used to investigate changes in the mean, vari-
22 ability and extremes of climate, as forced with predicted greenhouse gas (GHGs) concentrations
23 and aerosol emissions (Meehl et al. 2006). Several past studies have investigated global impacts
24 (Seneviratne et al. 2012), but studies addressing impacts at local and regional scales are less com-
25 mon. Although increased GHG concentrations have contributed to the observed intensification
26 of heavy precipitation events over the tropical ocean (Allan and Soden 2008) and the majority of
27 Northern Hemisphere overland areas (Min et al. 2011), these impacts are much more poorly un-
28 derstood at regional scales due to variability at finer spatial scales associated with the atmospheric
29 circulation (Trenberth 2011). As a consequence of this variability, confidence in the assessment of
30 regional extreme precipitation changes requires both high spatial resolution and a long integration
31 period, both of which can make the computational cost untenable for global simulations.

32 This issue of insufficient regional-scale climate information has been a major outstanding prob-
33 lem in climate science, as stakeholders and water managers typically require fine-scale information
34 on climate impacts in order to effectively develop adaptation and mitigation strategies. Dynamical
35 downscaling with regional climate models (RCMs) has been one of the few tools available to
36 ascertain the frequency, intensity, and duration of extreme events at the needed scales. By only
37 simulating a limited regional domain, RCMs better capture fine-scale dynamical features with
38 high horizontal resolution (Bell et al. 2004; Frei et al. 2006; Rauscher et al. 2010; Wehner 2013).
39 Higher resolution enables more accurate simulation of precipitation extremes, which are driven by
40 circulation patterns, cloudiness, land use, land/water contrast, snowpack and topography (Leung
41 et al. 2003a; Diffenbaugh et al. 2005; Salathé Jr et al. 2008; Wehner et al. 2010). Diffenbaugh et al.
42 (2005) studied both heat events and precipitation events over the contiguous United States using a
43 RCM configured at 25 km horizontal resolution, and demonstrated that fine-scale processes were
44 critical for accurate assessment of local- and regional-scale climate change vulnerability. Leung
45 et al. (2003b) showed that the higher-resolution RCMs yield more realistic precipitation patterns
46 and produce more frequent heavy precipitation over the western U.S. (WUS), consistent with ob-
47 servations. [Alan: Are there any newer studies? 2005 (Diffenbaugh) and 2003 (Leung) seem
48 pretty dated now.]

49 Despite their success, RCMs also have known issues associated with inconsistency between
50 the lateral forcing data and the driven RCM. The menu of physical parameterizations and tuning
51 parameters typically available to RCMs can also lead to over-tuning of the model for a partic-
52 ular geographic region or climatological field (McDonald 2003; Laprise et al. 2008; Mesinger
53 and Veljovic 2013). Consequently, there has been growing interest in variable-resolution enabled
54 GCMs (VRGCMs) to improve regional climate simulations. Unlike RCMs, which require GCM
55 data to drive the simulation at lateral boundaries, VRGCMs use a unified model with coarse global

resolution and enhanced resolution over a specific study region (Staniforth and Mitchell 1978; Fox-Rabinovitz et al. 1997). VRGCMs have demonstrated competitive ability for regional climate studies at a reduced computational cost, particular when compared to uniform-resolution GCMs (Fox-Rabinovitz et al. 2006; Rauscher et al. 2013).

In this paper, we utilize the recently developed variable-resolution option in the Community Earth System Model (VR-CESM). VR-CESM is based on the CESM (and its predecessor, the Community Climate System Model (CCSM)), a family of models that have been used for decades to study the global climate (Neale et al. 2010a; Hurrell et al. 2013). The overall performance of VR-CESM for modeling regional climate in the California and Nevada is detailed in Huang et al. (2016), where it was argued that VR-CESM has competitive biases in comparison to the Weather Research and Forecasting (WRF) model (a traditional RCM) and the uniform-resolution CESM, when evaluating against high-quality observations and reanalysis. VR-CESM has been used in a number of studies to simulate fine-scale atmospheric processes (Zarzycki et al. 2014, 2015; Rhoades et al. 2015).

This study focuses on changes in the character of precipitation over the 21st century within the WUS, as predicted from long-term ensemble runs conducted with VR-CESM with a local grid resolution of $\sim 0.25^\circ$. The WUS is known to be particularly vulnerable to hydrological extremes, particularly floods and droughts (Leung et al. 2003b; Caldwell 2010), and hosts a variety of local features and microclimates associated with its rough and varied topography. Simulations of the future climate are performed in accordance with the representative concentration pathway (RCP) 8.5 scenario, which describes a “business-as-usual” projection for GHGs (Riahi et al. 2011). In this study we focus singularly on the RCP 8.5 scenario because its mid-century results are similar to a more optimistic RCP2.6 scenario end-of-century. Simulations are further conducted in accordance with the Atmospheric Model Intercomparison Project (AMIP) protocol (Gates 1992), a widely-

80 used approach for climate model diagnosis, validation and intercomparison that imposes global
81 sea surface temperatures (SSTs) and sea ice. It is well-known that correctly simulating changes
82 to the spatial pattern of SSTs in state-of-the-art coupled GCMs remains a significant challenge
83 (Joseph and Nigam 2006; Stevenson 2012; Jha et al. 2014; Taschetto et al. 2014). However, by
84 constraining atmospheric boundary conditions at the sea surface, we avoid model biases that are
85 known to exist in the fully coupled configuration (Grodsy et al. 2012; Small et al. 2014) and
86 accept potential uncertainties associated with our choice of SSTs.

87 Changes in the character of precipitation, in terms of frequency and intensity, have been as-
88 sessed in our study from recent history through the end of the 21st century. A comprehensive
89 set of metrics for precipitation extremes have been evaluated from ensemble simulations over the
90 26-year periods corresponding to historical (1980-2005), mid-century (2025-2050) and end-of-
91 century (2075-2100). We hypothesize that spatial inhomogeneity in local geography and temper-
92 ature will also result in similarly inhomogeneous impacts on the precipitation field. We further
93 expect that teleconnections (specifically the El Niño-Southern Oscillation, ENSO) will have a
94 pronounced impact on precipitation features. Since only one SST dataset was used for this study,
95 we note that our projections are conditioned on a particular future character of ENSO. This is a
96 potentially large source of uncertainty, as at present there is no clear consensus on how ENSO
97 may behave under a warming climate (Fedorov and Philander 2000; Latif and Keenlyside 2009;
98 Guilyardi et al. 2009; Collins et al. 2010; DiNezio et al. 2012), and strengthening or weakening of
99 this pattern will have clear consequences for our results (as discussed in section 6d).

100 This work builds on a number of previous studies that have explored the projected future change
101 in WUS precipitation. For example, Kim (2005) applied downscaled climate change signals to se-
102 lected indicators, and concluded that global warming induced by increased CO₂ is likely to drive
103 increases in extreme hydrologic events in the WUS. Duffy et al. (2006) found that changes to

¹⁰⁴ mean precipitation predicted by the RCMs are not statistically significant compared to interannual
¹⁰⁵ variability in many regions over WUS, although there is little consistency among the different
¹⁰⁶ RCMs as to responses in precipitation to increased GHGs. Gao et al. (2015) pointed out a poten-
¹⁰⁷ tially large increase in atmospheric river events by the end of the 21st century under the RCP8.5
¹⁰⁸ scenario, with implications for large-scale and heavy precipitation events along the Pacific coast.

¹⁰⁹ This paper is structured as follows. Section 2 describes the model setup. Section 3 describes
¹¹⁰ the methodology and reference datasets employed. An assessment of the ability of the model to
¹¹¹ capture the climatology of the WUS is given in section 4. Results from the future mean climato-
¹¹² logical trend and projected changes to precipitation indices are in section 6. Section 7 summarizes
¹¹³ the main points of the study along with further discussion.

¹¹⁴ 2. Model Setup

¹¹⁵ CESM is a state-of-the-art Earth modeling framework, consisting of coupled atmosphere, ocean,
¹¹⁶ land and sea ice models (Neale et al. 2010b; Hurrell et al. 2013). In this study, the Community At-
¹¹⁷ mosphere Model version 5 (CAM5) (Neale et al. 2010b) and the Community Land Model version
¹¹⁸ 4.0 (Oleson et al. 2010) are used. CAM5 is configured with the Spectral Element (SE) dynamical
¹¹⁹ core, which is known for its conservation properties, accuracy and parallel scalability (Dennis et al.
¹²⁰ 2011; Taylor 2011) and incorporates the variable-resolution option (Zarzycki et al. 2014). CLM
¹²¹ is employed in the *unigrid* configuration, which allows the land model and atmospheric model to
¹²² utilize the same model grid so eliminates the need for interpolation. SSTs and sea ice, which are
¹²³ used to compute ocean-atmosphere fluxes, are prescribed in accordance with the AMIP protocol
¹²⁴ (Gates 1992). The variable-resolution mesh used for this study is depicted in Figure 1, in accord
¹²⁵ with our past studies (Rhoades et al. 2015; Huang et al. 2016; Huang and Ullrich 2016).

126 Simulations have been performed for the historical period (1979-2005, hereafter referred to as
127 hist) and for two future periods: 2024-2050 (hereafter referred to as mid) and 2074-2100 (hereafter
128 referred to as end). Daily output are recorded for each period on the native SE grid and then
129 remapped to a regional latitude-longitude mesh (Ullrich and Taylor 2015; Ullrich et al. 2016). For
130 purposes of analysis, the first year of each time period was discarded as a spin-up period to allow
131 adequate time for the initialized land and atmosphere to equilibrate. The 26-year duration was
132 chosen to provide an adequate sampling of annual variability for each time phase. As mentioned
133 earlier, GHG concentrations are set based on RCP8.5. Historical SSTs and sea ice are prescribed
134 at 1° resolution, as described by Hurrell et al. (2008). SSTs and sea ice for each future period are
135 developed from fully-coupled RCP 8.5 climate simulations with bias correction applied (Cecile
136 Hannay, personal communication). Annually-updated land surface datasets, which prescribe land-
137 use characteristics, are interpolated from 0.5° to the land model grid.

138 Ensemble runs are needed to ensure that the sample adequately accounts for climate variability,
139 especially for statistics associated with climatological extremes. However, the exact number of
140 ensemble members required is heavily dependent on the variability of the particular metric being
141 examined, and so no standard ensemble criteria exists. Deser et al. (2012b) suggest that around
142 3 ensemble runs are required to detect a significant epoch difference for JJA (June-July-August)
143 surface temperatures, whereas 10 to 30 ensemble members are needed for that for DJF (Dec.-Jan.-
144 Feb.) precipitation. In our study, the use of prescribed SSTs does reduce the intrinsic variability
145 of the climate system (see supplement), and so we found reasonably converged results with two
146 ensemble members for the historical period and four ensemble members for each future period.

¹⁴⁷ **3. Methodology**

¹⁴⁸ *a. Precipitation indices*

¹⁴⁹ Standard indices have been employed to characterize precipitation (Tebaldi et al. 2006; Zhang
¹⁵⁰ et al. 2011; Sillmann et al. 2013). In order to choose a comprehensive (but minimal) set that are
¹⁵¹ informative to stakeholders and water managers, indices from throughout the literature have been
¹⁵² assessed. The indices examined include those defined by the Expert Team on Climate Change De-
¹⁵³ tection and Indices (ETCCDI) (Karl et al. 1999) that are featured in earlier studies (Dulière et al.
¹⁵⁴ 2011; Sillmann et al. 2013; Diffenbaugh et al. 2005; Singh et al. 2013) and others such as return
¹⁵⁵ levels, dry spell and wet spell characteristics defined by either percentiles or by selected thresh-
¹⁵⁶ olds. The indices we have chosen for this study attempt to provide a relatively comprehensive
¹⁵⁷ characterization of precipitation, and are summarized in Table 1.

¹⁵⁸ [Paul: You should probably state at some point why you don't employ drought or dry spell
¹⁵⁹ indices]

¹⁶⁰ *b. Impacts of ENSO*

¹⁶¹ The impact of ENSO on precipitation is emphasized in our study due to its influence on precipi-
¹⁶² tation over a majority of our study area, particularly the southwest U.S. (Cayan et al. 1999; Zhang
¹⁶³ et al. 2010; Deser et al. 2012a; Yoon et al. 2015). The phase of ENSO (*i.e.* El Niño and La Niña)
¹⁶⁴ is identified each year using the Oceanic Niño Index (ONI), defined as the 3-month running means
¹⁶⁵ of SST anomalies in the Niño 3.4 region (covering 5N-5S, 120-170W based on NOAA (2013)).
¹⁶⁶ An El Niño or La Niña episode is said to occur when the ONI exceeds +0.5 or -0.5 for at least five
¹⁶⁷ consecutive months for a water year (*i.e.* from July to June) (NOAA 2013) (see the supplement).
¹⁶⁸ In order to adjust for the trend in the SST field associated with climate change, the anomaly is

169 computed against the detrended mean SSTs from the periods 1971-2000, 2020-2050 and 2070-
170 2100 for `hist`, `mid` and `end` respectively, using the aforementioned observed and predicted SST
171 datasets. As argued by Kao and Yu (2009), it may be desirable to use an extended Niño 3.4 region
172 to determine the phase of ENSO – however, when employing SST anomalies integrated over the
173 region 105-170W, we observed no significant impact on ONI statistics.

174 *c. Assessing statistical significance*

175 Student's t-test has been used to determine whether or not two datasets at each grid point are
176 statistically equivalent, if the sample population can be adequately described by a normal distri-
177 bution. The normality of a dataset is assessed under the Anderson-Darling test. When the sample
178 populations do not approximately follow a normal distribution, Mann-Whitney-Wilcoxon (MWW)
179 test is employed in lieu of the t-test. All these tests are evaluated at the 0.05 (α) significance level.
180 When comparing different time periods, statistical tests are conducted by treating all years from
181 all ensemble members as independent samples (26×2 sample years for `hist` and 26×4 sample
182 years for `mid` and `end`).

183 (add description of the supplement like what are included; see the `sst_enso.pdf`, mask the land
184 (over land, it should be the surface temperature.))

185 *d. Reference datasets*

186 Gridded observational datasets and reanalysis of the highest available quality, with comparable
187 horizontal resolutions to our VR-CESM simulations, are used for assessing the simulation qual-
188 ity. Multiple reference datasets are necessary due to the underlying uncertainty in interpolating
189 precipitation fields. The three datasets employed are as follows:

190 **UW Gridded Data:** The 0.125° UW daily gridded meteorological data is obtained from
191 the Surface Water Modeling group at the University of Washington, covering the period
192 1949-2010 (Maurer et al. 2002; Hamlet and Lettenmaier 2005). The UW dataset imposes
193 topographic corrections by forcing the long-term average precipitation to match that of the
194 Parameter-elevation Regressions on Independent Slopes Model (PRISM) dataset.

195 **National Centers for Environmental Prediction (NCEP) Climate Prediction Center**
196 **(CPC):** The 0.25° CPC daily dataset provides gauge-based analysis of daily precipitation cov-
197 ering the period 1948-2006. It is a unified precipitation product that covers the Conterminous
198 United States and amalgamates a number of data sources at CPC via optimal interpolation
199 objective analysis.

200 **North American Regional Reanalysis (NARR):** NARR is a ~ 32 km high-resolution reanal-
201 ysis product with 3-hourly output produced by NCEP via dynamical downscaling over North
202 America and covering the period 1979-present (Mesinger et al. 2006).

203 **4. Assessment of Precipitation Character in VR-CESM**

204 Before proceeding, we assess the ability of VR-CESM to represent the character of precipitation
205 over the WUS. The indices defined in Table 1 are depicted in Figures 2, 3 and 4 for VR-CESM
206 and each of the reference datasets over the historical period (1980-2005). We assume equal con-
207 fidence in each of the reference datasets, and use Student's t-test (with UW, CPC and NARR as
208 the three statistical samples) to identify regions where VR-CESM deviates significantly from the
209 reference mean. Regions where differences are statistically significant in the VR-CESM dataset
210 are identified with stippling.

211 Overall, VR-CESM largely captures the spatial patterns of precipitation and its indices. As ex-
212 pected, the majority of precipitation is distributed along the northwest coastal area and the moun-
213 tainous regions of the Cascades and the Sierra Nevada. Nonetheless, several apparent biases are
214 present:

215 First, VR-CESM significantly overestimates Pr over dry regions with differences between 0.2
216 mm to 1.5 mm, and over the eastern flank of the Cascades and on both sides of the Sierra Nevada
217 (with relative differences reaching 50%-150%). As with many regional models, VR-CESM is
218 “dreary” and exhibits too many precipitation days (R_{1mm} , $Pr \geq 1$ mm/day and R_{5mm} , 1 mm/day \leq
219 $Pr \leq 5$ mm/day) (see Figure 3) [citation needed]. Nonetheless, over most regions the relative con-
220 tribution of each precipitation frequency subset to total precipitation (F_{1mm} , F_{5mm} , F_{10mm} ,
221 F_{20mm} and F_{40mm}) agrees well, suggesting that the frequency distribution describing precipita-
222 tion intensity is accurately simulated almost everywhere.

223 Second, the spatial pattern of precipitation intensity (SDII) agrees well between VR-CESM
224 and references with agreement everywhere except in the Great Plains (the eastern edge of our
225 domain) and in California’s Central Valley. The Great Plains is not a focus of this study, but
226 the suppressed intensity is primarily during the warm season (April-September) and so likely
227 represents a failure of the convection scheme to adequately simulate variability in this region.
228 This bias is also observed in 0.25° uniform-resolution CESM simulations (Small et al. 2014), and
229 so is not a symptom of the eastern edge of the variable-resolution transition region.

230 However, the grossly exaggerated intensity over the western flank of the Sierra Nevada through
231 California’s Central Valley does merit some additional discussion. Here, the overestimation of pre-
232 cipitation and enhanced intensity is associated with too many extreme precipitation events ($Pr > 20$
233 mm/day) (see Figure 4, F_{40mm} and F_{xmm}). This bias is related to exaggerated orographic uplift
234 (upslope winds, not shown) and triggers a dry bias along the eastern flank of the Sierras. Similar

235 biases in simulating extreme precipitation over topographically complex regions have also been
236 found in high-resolution RCM simulations, and have been primarily attributed to excessively strong
237 winds (Walker and Diffenbaugh 2009; Singh et al. 2013). This issue may be further impacted by
238 the diagnostic treatment of precipitation in CAM5 (Morrison and Gettelman 2008; Gettelman et al.
239 2008).

240 The representation of precipitation in VR-CESM over California was also discussed in Huang
241 et al. (2016), where it was observed that VR-CESM simulations at 0.25° adequately represented
242 regional climatological patterns with high spatial correlation. VR-CESM demonstrated compa-
243 rable performance to WRF at 27 km (which was forced with ERA-Interim reanalysis), but still
244 overestimated overall winter precipitation compared to reference datasets (by about 25%-35%),
245 with the largest differences over the western edge of the Sierra Nevada. This bias is not allevi-
246 ated by simply increasing the spatial resolution, as experimental VR-CESM simulations at 14km,
247 7km and 3.5km show only modest improvement (Alan M. Rhoades, personal communication).
248 This suggests that the bias might be related with more complex dynamic processes rather than
249 treatment of the orographic effects.

250 CESM at 1° resolution was also assessed in order to better understand the impacts of resolu-
251 tion. We find that precipitation patterns over complex topography are poorly represented in the 1°
252 dataset and do not capture the spatial patterns induced by orographic effects. Over the Cascades
253 and Sierra Nevada, total precipitation is grossly underestimated by 1° CESM, when compared to
254 VR-CESM, gridded and reanalysis datasets (see the supplement [[Point to exact figure](#)]). Precip-
255 itation has otherwise been smoothed out over the coastal areas and the mountainous regions of
256 the northwest U.S when simulated with CESM at coarse resolution. This result clearly under-
257 scores the benefits of high resolution (particularly the representation of topography) in simulating
258 precipitation features. Results are also provided in the supplement for the output from a globally-

uniform CESM run at 0.25° spatial resolution with the finite volume (FV) dynamical core (Wehner et al. 2014), which exhibits similar performance to VR-CESM (see the supplement [Point to exact figure]). Overall, 0.25° resolution appears to provide the best tradeoff between accuracy and computational cost, as coarser resolution does not correctly represent precipitation features and higher resolution does not appear to substantially improve model accuracy.

We have also assessed the impact of the ENSO signal within the historical VR-CESM runs by differencing the precipitation fields between the warm phase (i.e. El Niño) and cool phase (i.e. La Niña), compared to references (see the supplement). ENSO exhibits a weaker signal for observational precipitation, compared to VR-CESM, which might suggest that the model exaggerates ENSO's impact on precipitation, especially over the northwest U.S. The improvement of ENSO in the model is directly proportional to the representation of ENSO-forced precipitation anomalies (AchutaRao and Sperber 2006).

5. Drivers of Climatological Precipitation Change

The remainder of this paper now focuses on model predictions of change over the 21st century. Precipitation has been observed and modeled to be modified in character at both global and regional scales under climate change. The observed intensification of heavy precipitation events over the recent past for the majority of Northern Hemisphere land areas is primarily attributed to increases in GHGs (Min et al. 2011). GHGs drive radiative changes in the lower troposphere, increase SSTs and lead to increased evaporation, all of which then impact the character of precipitation events (Allen and Ingram 2002; Sugi and Yoshimura 2004). Several studies have argued that precipitation extremes will intensify continuously through the end of 21st century in both dry and wet regions, although the extent of this change will be spatially heterogeneous (Donat et al. 2016).

282 In accordance with the Clausius-Clapeyron (C-C) relationship, saturation vapor pressure in the
283 atmosphere is expected to increase by $\sim 7\%$ for each 1°C increase in temperature (Allan and So-
284 den 2008). As long as a source of water vapor is present, a corresponding increase in atmospheric
285 water vapor content is expected. Naturally, evaporation over the ocean will increase with climate
286 warming, but increases in water vapor content over land may be constrained by soil moisture
287 (Cayan et al. 2010). When specific humidity is high, heavy rain events become more probable,
288 even if total precipitation is decreasing (Trenberth 2011). This suggests that global total precipi-
289 tation is expected to increase at a slower rate than precipitation extremes (Allan and Soden 2008).
290 In accordance with previous studies (e.g. (Allan and Soden 2008; O’Gorman and Schneider 2009;
291 Min et al. 2011)), changes to extreme precipitation follow the C-C relationship more closely than
292 total precipitation amount (Trenberth et al. 2003). However, there is still substantial uncertainty
293 for the magnitude of the change, since precipitation extremes are also dependent on factors such
294 as the vertical velocity profile and temperature (O’Gorman and Schneider 2009).

295 With overland water vapor constrained by soil moisture content, changes to moderate or heavy
296 precipitation events over the WUS are mainly the result of increased large-scale vapor transport
297 from the eastern Pacific Ocean rather than directly from evaporation, typically associated with
298 atmospheric rivers (ARs) and/or orographic uplift (Trenberth et al. 2003; Neiman et al. 2008).
299 Warming may lead to enhancement of the storm track, which would increase ARs along the U.S.
300 west coast with increased air water vapor content in the future (Dettinger 2011; Gao et al. 2015).
301 In the following sections, both the mean changes of precipitation and distributions of both non-
302 extreme and extreme events are investigated as projected by the VR-CESM model under climate
303 forcing.

304 The precipitation of the WUS has strong inter-annual variability caused by large-scale atmo-
305 spheric circulation mainly associated with the ENSO (Leung et al. 2003b). As a significant

306 driver of precipitation, ENSO modulates the storm track behavior over western U.S. with a north-
307 west/southwest precipitation dipole (Gershunov and Barnett 1998), as discussed in d. The pro-
308 jected SSTs used in this study emerge from one possible outcome for ENSO. However, there is
309 still substantial uncertainty regarding how El Niño will change under global warming (Fedorov
310 and Philander 2000; Guilyardi et al. 2009), which is a source of uncertainty in our results. Capo-
311 tondi (2013) showed that the diversity of El Niño characteristics in CCSM4 is comparable to what
312 was found in observations, although, as found by Deser et al. (2012c), the overall magnitude of
313 ENSO in CCSM4 [Paul: was this changed at all in CESM1?] is overestimated by 30% over the
314 preindustrial time period.

315 **6. Results**

316 *a. Mean climatology*

317 The mean climatological changes in VR-CESM across time periods are depicted in Figure 5.
318 Since the character of WUS precipitation has a strong seasonal contrast, changes to mean precipi-
319 tation, near-surface temperature and near-surface relative humidity are depicted for what we refer
320 to as the cool season (October to March) and the warm season (April to September).

321 As a result of enhanced GHG concentrations, mean annual near-surface temperature (T_{avg})
322 increases by about 1.5 to 2 K from hist to mid and about 4 to 6 K from mid to end. Despite the
323 large spatial variation in mean seasonal temperatures, the observed change to mean temperature is
324 fairly uniform, particularly over the ocean and in coastal regions. Away from the coast there is a
325 weak gradient in the temperature change field, with the largest increase in temperatures occurring
326 towards the northeast during the cool season and towards the north during the warm season. The

327 increase in temperature is also about 0.5K and 1.0K larger during the warm season compared to
328 the cool season for mid and end, respectively.

329 Overall, future RH is constrained closely to hist since it is governed by competing increases in
330 temperature and atmospheric water vapor content. Although RH increases monotonically over the
331 ocean in response to increased evaporation, over land the character is more heterogeneous: In gen-
332 eral, RH tends to increase in regions where Tavg increase is constrained below \sim 2 K, but decrease
333 when Tavg anomaly exceeds \sim 2 K. The decrease in these regions is on the order of 2% and 3-6%,
334 compared to mid and end respectively. In fact, trends in RH are spatially consistent with tempera-
335 ture increase but opposite in magnitude with a spatial correlation coefficient of approximately 0.8.
336 This suggests that continental evaporation and oceanic water vapor transport are insufficient vapor
337 sources when temperature reaches a certain level, consistent with the observation of Joshi et al.
338 (2008). This effect has also been observed in results by Rowell and Jones (2006) over continental
339 and southeastern Europe and Simmons et al. (2010) over low-latitude and midlatitude land areas.

340 In response to these changes to temperature and RH, from hist to mid mean precipitation over
341 the entire domain exhibited a 0.2-0.6 mm/day increase during the cool season. The largest changes
342 were over northwest, where cool-season precipitation emerges from large-scale patterns (namely,
343 atmospheric rivers and associated storm systems)(Trenberth et al. 2003; Neiman et al. 2008). Over
344 the warm season, where precipitation in the WUS is primarily from convection, the increase was
345 around 0.2 mm/day through the intermountain west and southwest with drying through the north-
346 west (a decrease in mean precipitation of 0.2 mm/day). These trends largely hold and intensify
347 through end, except in the intermountain west and southwest regions where precipitation again
348 falls to historical levels. Statistical significance of these results is depicted in Figure 6.

349 The increase in cool season precipitation in the Northwest is largely driven by increased inte-
350 grated vapor transport (IVT) (see Figure 8a,b) during extreme precipitation events. IVT is par-

ticularly useful for understanding extreme precipitation events that arise from large-scale meteorological features (Ralph et al. 2004; Leung and Qian 2009; Dettinger 2011). IVT is composed of absolute humidity and wind velocity, which are both impacted by the climate change signal. To understand how these two factors respond to the climate change signal and contribute to the increase in IVT, specific humidity and wind vectors are plotted in Figure 8b. Over the eastern Pacific, we observe increases in both water vapor content and wind speed, which are in turn responsible for increases to IVT in the Pacific Northwest. However, over the continent we see a weakening of the westerlies overland driven by a reduced meridional temperature contrast. The increased cool-season IVT does not manifest strongly along the Pacific coast off of California, where IVT is much smaller on average and is primarily modulated by ENSO.

Changes in precipitation over the Intermountain West and Southwest during the warm season are primarily associated with convective processes and so are directly impacted by variations in RH. As shown in Figure 5, RH increases through mid-century in this region (although with modest significance) and then significantly decreases through end-of-century over most the study area (except over where soil moisture was already low in hist). This results in a modest increase in precipitation through mid-century followed by a return to historical precipitation amounts by end-of-century. Further climate warming is expected to further decrease RH and drive increased aridity in this region.

b. Precipitation indices

We now analyze observed changes to the precipitation indices given in Table 1. For each index, the change for each period, yearly averaged over all ensemble members are plotted in Figure 6 (for the indices that quantify precipitation days) and Figure 7 (for the indices describing precipitation amounts).

374 On comparing `hist` and `mid`, it is clear that the number of rainy days and frequency of non-
375 extreme precipitation events (≤ 10 mm/day) have increased significantly (about 10-15%) over the
376 southwest and intermountain west, which is less obvious between `mid` and `end`. On the contrary,
377 the frequency of non-extreme precipitation have decreased significantly over the northwest region
378 and the eastern areas of the Montana, Wyoming and Oregon (by about 10%). The increase in
379 the frequency of these non-extreme precipitation events explain the observed change to mean
380 precipitation exhibited in Figure 5, and are largely associated with warm season mesoscale storm
381 systems.

382 Although essentially all regions exhibit an increase in the most extreme precipitation events (Pr
383 ≥ 10 mm/day), this increase is only statistically significant through the intermountain west and
384 in the Pacific northwest (for $Pr \geq 20$ mm/day). When comparing `mid` to `end`, there is a clear
385 and significant increase in extreme precipitation events over the northwest coast (~ 20 -30%) and
386 eastern flank of the Cascades ($> 40\%$). This result is consistent with the result of Dominguez
387 et al. (2012), who observe a robust increase in winter precipitation extremes toward the latter half
388 of the 21st century with an ensemble of RCMs. The increase in the northwest is accompanied by
389 a decrease in non-extreme precipitation days, indicative of drying over the warm season.

390 [Paul: For each region it would be extremely valuable to include changes to the return frequency
391 of the most extreme events – i.e. in the Northwest a five-year storm becomes a two-year storm]

392 Notably, our results show no significant change in precipitation character is predicted for Cali-
393 fornia. In fact, the precipitation signal under a warmer climate is more ambiguous for California
394 (Neelin et al. 2013) in light of the extreme variability of the region on interannual time scales
395 (Dettinger 2011). Kim (2005) found that under global warming, heavy precipitation events in-
396 crease in frequency in the mountainous regions of the northern California Coastal Range and the
397 Sierra Nevada. However, our results show a small decrease in extreme precipitation over the Sierra

398 Nevada (although the decrease is not statistically significant). This leads us to the likely conclu-
399 sion (particularly in light of VR-CESM's own biases in this region) that projections in this region
400 are highly dependent on model formulation.

401 For the most extreme precipitation events ($\text{Pr} \geq 40 \text{ mm/day}$), there is a statistically significant
402 increase along the northwest coast ($\geq 60\%$), the Cascades ($\sim 50\%$) and Northern Rockies ($\geq 60\%$)
403 by end-of-century. Significant increases are also apparent along the Klamath range in California
404 of about 20-40% from hist to end. Changes in accumulated precipitation for these events are con-
405 sistent with the change in their frequency (see Figure 7). With a projected increase of temperatures
406 in this region of 4-5 K over the cool season, this increase is in excess of the 7% per degree change
407 that would be anticipated from the C-C relationship (Figure 8a). In this case, the probable cause
408 of this excess is due to the intensification of the storm track along the coast discussed in section a.

409 *c. Regional precipitation frequency distributions*

410 To further investigate the regional heterogeneity of changing precipitation, frequency distribu-
411 tions of daily rainfall for rainy days are plotted in Figure 9 for (a) the Pacific Northwest, including
412 Washington and Oregon, (b) California, (c) the Intermountain West, including Nevada and Utah
413 and (d) the Southwest, including Arizona and New Mexico [Paul: Region labels need to be moved
414 earlier in the text, and we probably need a figure to identify how we refer to regions (add Northern
415 Rockies (Idaho, Montana and Wyoming) and Great Plains (Dakotas through north Texas). Fre-
416 quency plots are developed using simulation outputs at all grid points within each region. [Paul:
417 As discussed, need to split these plots into non-extreme / extreme] Over the Northwest, precip-
418 itation intensifies with upper tail going more extreme in the future, especially during end. No
419 apparent changes can be observed for the California region, except with more extreme upper tail
420 for Pr exceeding 100 mm/day during end, which is due to the increased precipitation extremes

over the northern California as shown in Figure 7. Over the inter-mountainous region, similar trends of changes can be seen as the northwest area, with intensified mean and extreme precipitation. For the southwest area, precipitation tends to be more extreme with a moderate level, although no notable difference exists between mid and end.

d. Disentangling the direct climate signal from ENSO and PDO

As discussed earlier, this study assumes a fixed pattern of SSTs that is consistent across all ensemble members and incorporates certain assumptions on the character of ENSO through the end-of-century that arise from the coupled model. The phase of ENSO is well known to have important repercussions for precipitation extremes (Larkin and Harrison 2005; Allan and Soden 2008; Maloney et al. 2014; Yoon et al. 2015). In particular, Cai et al. (2014) found a significant increase in extraordinary precipitation events through the eastern Pacific Ocean in the 21st century within the CMIP5 ensemble, associated with increasing frequency of extreme El Niño events due to greenhouse warming. To better understand how ENSO has impacted our results, we now turn our attention to understanding how precipitation extremes behave in response to the phase of ENSO.

In our study, mean SSTs over the Niño 3.4 region are 26.83, 28.62 and 30.54°C for hist, mid and end respectively. Based on the ONI index values, the mean SST anomalies are 1.38, 1.71 and 2.30 K during El Niño years, and -1.16, -1.62 and -1.43 K during La Niña years, again for hist, mid and end. It is apparent within that within this dataset the magnitude of SST anomalies associated with ENSO has intensified. SST anomalies of each year and each month, and their associated spatial pattern when averaged over the warm and cool phases of ENSO can be found in the supplement, suggesting an increasing frequency of El Niño through mid and an almost doubled frequency of La Niña during mid and end compared to the hist.

444 [Huang: As SSTs increase in the future, is not it normal for the anomaly of ENSO to be increased
445 to compensate the changes of water vapor capacity? Might email Neale about this]

446 Differences in mean precipitation and associated indices taken between the warm phase (i.e.
447 El Niño) and cool phase (i.e. La Niña) of ENSO are provided in Figure 10 for the cool seasons
448 from hist, mid and end. During the El Niño phase, intensified mean precipitation is expected
449 over California and the southwest (Hamlet and Lettenmaier 2007), accompanied by reduced pre-
450 cipitation intensity over the northwest. In the La Niña phase, this pattern is reversed, with wetter
451 conditions in the northwest and a drier southwest. Consequently, ENSO is associated with a
452 northwest/southwest precipitation dipole, triggered by ENSO's modification of the storm track
453 (Gershunov and Barnett 1998; Leung et al. 2003b), along with modulation of the enhanced pre-
454 cipitation variability (Cayan et al. 1999; Kahya and Dracup 1994). Strengthening storm patterns
455 associated with ENSO are also found by Maloney et al. (2014) over California using CMIP5
456 output under RCP8.5. This dipole is also apparent in the frequency of rainy days and extreme
457 precipitation events.

458 The impact of ENSO can also be seen in the IVT difference that arises between El Niño and
459 La Niña phases in each time period (see Figure 11) and the accompanying 850 hPa wind patterns.
460 During the El Niño phase, there is an increase in on-shore moisture flux over California that
461 triggers a returning circulation through the northwest. This suggests that understanding moisture
462 flux regulation from ENSO is a very important contributor to the character of future precipitation
463 extremes.

464 Based on the above results, it is apparent that the magnitude of the effects of ENSO is compa-
465 rable or even higher than the impacts of climate forcing – that is, shifts in the future character of
466 ENSO would have more dire implications for precipitation extremes than shifts in mean climato-
467 logical forcing. To investigate this further, linear regression has applied at each grid point using

468 a simple linear model that incorporates the phase of ENSO (using the Niño 3.4 SST anomaly)
469 and the underlying climate forcing (from mean GHG concentration). The precipitation indices are
470 used as response variables. The significance of these two factors was then obtained from ANOVA
471 (analysis of variance) output (see the supplement [Paul: Point to lm_fit_pvalue]). The magnitude
472 of the response associated with each factor was also computed (see the supplement [Paul: Point
473 to wd_lmfit_coef_enso_ghg]). As expected, the ENSO forcing matches most closely with the dif-
474 ference between El Niño and La Niña (see Figure 11). Hence, we observe that ENSO is a major
475 driver of precipitation character through California, the intermountain west and the southwest and
476 does have an impact on mean precipitation through the Cascades. In contrast, the impacts of cli-
477 mate forcing are visually similar to the pattern of the difference between the different time periods
478 (see Figure 6), and primarily impacts both extreme and non-extreme precipitation in the northwest
479 and intermountain west.

480 We have also assessed the impacts of the Pacific Decadal Oscillation (PDO) on precipitation and
481 observed only a weak correlation between the PDO pattern and precipitation. That is, precipita-
482 tion features did not change substantially between the cool phase or warm phase of PDO when
483 examining hist data. However, when in phase with ENSO, PDO did have a notable impact over
484 the northwest. This coupled effect has been found by previous studies Gershunov and Barnett
485 (1998), who observed that ENSO and PDO can “reinforce” each other, with PDO responding to
486 the same internal atmospheric variability as ENSO (Pierce 2002). In our simulations, there were
487 roughly an equal number of positive PDO years and negative PDO years in the data from each
488 time period, but since SSTs were fixed among ensemble members, the 26 year simulation period
489 might be insufficient to account for the variability of PDO. Therefore, in this study we draw no
490 conclusions on the impact of PDO.

491 **7. Discussion and Summary**

492 The increased cool season precipitation extremes tend to result in higher runoff events over
493 the northwest U.S., which are in turn associated with a greater chance of flooding and a loss of
494 snowpack. A decrease in counts of rainy days during the warm season over central and southern
495 California, though small in magnitude, will probably intensify the drought condition due to the
496 deficit of soil moisture with higher evapotranspiration caused by the warmer climate in the future
497 Cayan et al. (2010); Bell et al. (2004).

498 (Summary is to be added once the main content have been settled down The contribution of
499 human-induced increases in greenhouse gases to the character of precipitation is confounded by
500 patterns of variability in the atmospheric circulation. Consistent with previous studies, changes
501 in more extreme precipitation follow the Clausius-Clapeyron relationship more closely than total
502 precipitation amount. The changes of the strength of ENSO remains uncertain. However, the char-
503 acter of ENSO appears to be the largest factor in understanding changing precipitation extremes
504 in the U.S. West.)

505 Notes for the summary:

506 • Northwest: Increase in extreme precipitation events (state return time of 20mm/day and
507 40mm/day events) accompanied by a substantial moistening of the cool season, even though
508 total precipitation days doesn't change. This is driven by increased IVT over the eastern
509 Pacific. Increased drying over the warm season driven by a reduction in RH.

510 • California: No clear climate signal in mean precipitation or extremes. Precipitation in this
511 area is dominated by interannual variability, primarily associated with ENSO.

- 512 ● Intermountain West and Southwest: Increase in warm season RH through mid-century fol-
513 lowed by a reduced RH through end-of-century. Nonetheless accompanied by a statistically
514 significant increase in Pr and non-extreme rainy days due to increased convection (?)

515 *Acknowledgments.* The authors would like to thank Michael Wehner for sharing the dataset and
516 many suggestions. The authors also want to thank Alan M. Rhoades for providing the simulation
517 output. We acknowledge the substantial efforts behind the datasets used in this study, including
518 UW, NCDC and NARR. The simulation data used is available by request at xyhuang@ucdavis.edu.
519 This project is supported in part by the xxx and by the xxx.

520 References

- 521 AchutaRao, K., and K. R. Sperber, 2006: Enso simulation in coupled ocean-atmosphere models:
522 are the current models better? *Climate Dynamics*, **27** (1), 1–15.
- 523 Allan, R. P., and B. J. Soden, 2008: Atmospheric warming and the amplification of precipitation
524 extremes. *Science*, **321** (5895), 1481–1484.
- 525 Allen, M. R., and W. J. Ingram, 2002: Constraints on future changes in climate and the hydrologic
526 cycle. *Nature*, **419** (6903), 224–232.
- 527 Bell, J. L., L. C. Sloan, and M. A. Snyder, 2004: Regional changes in extreme climatic events: a
528 future climate scenario. *Journal of Climate*, **17** (1), 81–87.
- 529 Cai, W., and Coauthors, 2014: Increasing frequency of extreme el niño events due to greenhouse
530 warming. *Nature climate change*, **4** (2), 111–116.
- 531 Caldwell, P., 2010: California wintertime precipitation bias in regional and global climate models.
532 *Journal of Applied Meteorology and Climatology*, **49** (10), 2147–2158.

- 533 Capotondi, A., 2013: Enso diversity in the ncar ccsm4 climate model. *Journal of Geophysical*
534 *Research: Oceans*, **118 (10)**, 4755–4770.
- 535 Cayan, D. R., T. Das, D. W. Pierce, T. P. Barnett, M. Tyree, and A. Gershunov, 2010: Future
536 dryness in the southwest us and the hydrology of the early 21st century drought. *Proceedings of*
537 *the National Academy of Sciences*, **107 (50)**, 21 271–21 276.
- 538 Cayan, D. R., K. T. Redmond, and L. G. Riddle, 1999: ENSO and hydrologic extremes in the
539 western United States*. *Journal of Climate*, **12 (9)**, 2881–2893.
- 540 Collins, M., and Coauthors, 2010: The impact of global warming on the tropical pacific ocean and
541 el niño. *Nature Geoscience*, **3 (6)**, 391–397.
- 542 Dennis, J., and Coauthors, 2011: CAM-SE: A scalable spectral element dynamical core for the
543 Community Atmosphere Model. *International Journal of High Performance Computing Appli-*
544 *cations*, 1094342011428142.
- 545 Deser, C., R. Knutti, S. Solomon, and A. S. Phillips, 2012a: Communication of the role of natural
546 variability in future north american climate. *Nature Climate Change*, **2 (11)**, 775–779.
- 547 Deser, C., A. Phillips, V. Bourdette, and H. Teng, 2012b: Uncertainty in climate change projec-
548 tions: the role of internal variability. *Climate Dynamics*, **38 (3-4)**, 527–546.
- 549 Deser, C., and Coauthors, 2012c: Enso and pacific decadal variability in the community climate
550 system model version 4. *Journal of Climate*, **25 (8)**, 2622–2651.
- 551 Dettinger, M., 2011: Climate change, atmospheric rivers, and floods in california—a multimodel
552 analysis of storm frequency and magnitude changes1. Wiley Online Library.

- 553 Diffenbaugh, N. S., J. S. Pal, R. J. Trapp, and F. Giorgi, 2005: Fine-scale processes regulate the
554 response of extreme events to global climate change. *Proceedings of the National Academy of*
555 *Sciences of the United States of America*, **102** (44), 15 774–15 778.
- 556 DiNezio, P. N., B. P. Kirtman, A. C. Clement, S.-K. Lee, G. A. Vecchi, and A. Wittenberg, 2012:
557 Mean climate controls on the simulated response of enso to increasing greenhouse gases. *Journal*
558 *of Climate*, **25** (21), 7399–7420.
- 559 Dominguez, F., E. Rivera, D. Lettenmaier, and C. Castro, 2012: Changes in winter precipitation
560 extremes for the western united states under a warmer climate as simulated by regional climate
561 models. *Geophysical Research Letters*, **39** (5).
- 562 Donat, M. G., A. L. Lowry, L. V. Alexander, P. A. OGorman, and N. Maher, 2016: More extreme
563 precipitation in the world’s dry and wet regions. *Nature Climate Change*.
- 564 Duffy, P., and Coauthors, 2006: Simulations of present and future climates in the western United
565 States with four nested regional climate models. *Journal of Climate*, **19** (6), 873–895.
- 566 Duli  re, V., Y. Zhang, and E. P. Salath   Jr, 2011: Extreme Precipitation and Temperature over the
567 US Pacific Northwest: A Comparison between Observations, Reanalysis Data, and Regional
568 Models*. *Journal of Climate*, **24** (7), 1950–1964.
- 569 Easterling, D. R., G. A. Meehl, C. Parmesan, S. A. Changnon, T. R. Karl, and L. O. Mearns, 2000:
570 Climate extremes: observations, modeling, and impacts. *science*, **289** (5487), 2068–2074.
- 571 Fedorov, A. V., and S. G. Philander, 2000: Is el ni  o changing? *Science*, **288** (5473), 1997–2002.
- 572 Fox-Rabinovitz, M., J. C  te, B. Dugas, M. D  qu  , and J. L. McGregor, 2006: Variable resolution
573 general circulation models: Stretched-grid model intercomparison project (SGMIP). *Journal of*
574 *Geophysical Research: Atmospheres (1984–2012)*, **111** (D16).

- 575 Fox-Rabinovitz, M. S., G. L. Stenchikov, M. J. Suarez, and L. L. Takacs, 1997: A finite-difference GCM dynamical core with a variable-resolution stretched grid. *Monthly weather review*, **125** (11), 2943–2968.
- 576
- 577
- 578 Frei, C., R. Schöll, S. Fukutome, J. Schmidli, and P. L. Vidale, 2006: Future change of precipitation extremes in Europe: Intercomparison of scenarios from regional climate models. *Journal of Geophysical Research: Atmospheres (1984–2012)*, **111** (D6).
- 579
- 580
- 581 Gao, Y., J. Lu, L. R. Leung, Q. Yang, S. Hagos, and Y. Qian, 2015: Dynamical and thermodynamical modulations on future changes of landfalling atmospheric rivers over western north america. *Geophysical Research Letters*, **42** (17), 7179–7186.
- 582
- 583
- 584 Gates, W. L., 1992: AMIP: The Atmospheric Model Intercomparison Project. *Bulletin of the American Meteorological Society*, **73**, 1962–1970.
- 585
- 586 Gershunov, A., and T. P. Barnett, 1998: Interdecadal modulation of enso teleconnections. *Bulletin of the American Meteorological Society*, **79** (12), 2715–2725.
- 587
- 588 Gettelman, A., H. Morrison, and S. J. Ghan, 2008: A new two-moment bulk stratiform cloud microphysics scheme in the Community Atmosphere Model, version 3 (CAM3). Part II: Single-column and global results. *Journal of Climate*, **21** (15), 3660–3679.
- 589
- 590
- 591 Grodsky, S. A., J. A. Carton, S. Nigam, and Y. M. Okumura, 2012: Tropical atlantic biases in ccsm4. *Journal of Climate*, **25** (11), 3684–3701.
- 592
- 593 Guilyardi, E., A. Wittenberg, A. Fedorov, M. Collins, C. Wang, A. Capotondi, G. J. Van Oldenborgh, and T. Stockdale, 2009: Understanding el niño in ocean-atmosphere general circulation models. *Bulletin of the American Meteorological Society*, **90** (3), 325.
- 594
- 595

- 596 Hamlet, A. F., and D. P. Lettenmaier, 2005: Production of Temporally Consistent Gridded Precipi-
597 tation and Temperature Fields for the Continental United States*. *Journal of Hydrometeorology*,
598 **6** (3), 330–336.
- 599 Hamlet, A. F., and D. P. Lettenmaier, 2007: Effects of 20th century warming and climate variability
600 on flood risk in the western us. *Water Resources Research*, **43** (6).
- 601 Hegerl, G. C., F. W. Zwiers, P. A. Stott, and V. V. Kharin, 2004: Detectability of anthropogenic
602 changes in annual temperature and precipitation extremes. *Journal of Climate*, **17** (19), 3683–
603 3700.
- 604 Huang, X., A. M. Rhoades, P. A. Ullrich, and C. M. Zarzycki, 2016: An evaluation of the vari-
605 able resolution-cesm for modeling california’s climate. *Journal of Advances in Modeling Earth
606 Systems*.
- 607 Huang, X., and P. A. Ullrich, 2016: Irrigation impacts on california’s climate with the variable-
608 resolution cesm. *Journal of Advances in Modeling Earth Systems*.
- 609 Hurrell, J. W., J. J. Hack, D. Shea, J. M. Caron, and J. Rosinski, 2008: A new sea surface temper-
610 ature and sea ice boundary dataset for the Community Atmosphere Model. *Journal of Climate*,
611 **21** (19), 5145–5153.
- 612 Hurrell, J. W., and Coauthors, 2013: The community earth system model: A framework for col-
613 laborative research. *Bulletin of the American Meteorological Society*, **94** (9), 1339–1360.
- 614 Jha, B., Z.-Z. Hu, and A. Kumar, 2014: Sst and enso variability and change simulated in historical
615 experiments of cmip5 models. *Climate dynamics*, **42** (7-8), 2113–2124.
- 616 Joseph, R., and S. Nigam, 2006: Enso evolution and teleconnections in ipcc’s twentieth-century
617 climate simulations: Realistic representation? *Journal of Climate*, **19** (17), 4360–4377.

- 618 Joshi, M. M., J. M. Gregory, M. J. Webb, D. M. Sexton, and T. C. Johns, 2008: Mechanisms for
619 the land/sea warming contrast exhibited by simulations of climate change. *Climate Dynamics*,
620 **30** (5), 455–465.
- 621 Kahya, E., and J. A. Dracup, 1994: The influences of type 1 el nino and la nina events on stream-
622 flows in the pacific southwest of the united states. *Journal of Climate*, **7** (6), 965–976.
- 623 Kao, H.-Y., and J.-Y. Yu, 2009: Contrasting eastern-pacific and central-pacific types of enso.
624 *Journal of Climate*, **22** (3), 615–632.
- 625 Karl, T. R., N. Nicholls, and A. Ghazi, 1999: Clivar/gcos/wmo workshop on indices and indicators
626 for climate extremes workshop summary. *Weather and Climate Extremes*, Springer, 3–7.
- 627 Kharin, V. V., F. W. Zwiers, X. Zhang, and G. C. Hegerl, 2007: Changes in temperature and
628 precipitation extremes in the IPCC ensemble of global coupled model simulations. *Journal of*
629 *Climate*, **20** (8), 1419–1444.
- 630 Kim, J., 2005: A projection of the effects of the climate change induced by increased co2 on
631 extreme hydrologic events in the western us. *Climatic Change*, **68** (1-2), 153–168.
- 632 Laprise, R., and Coauthors, 2008: Challenging some tenets of regional climate modelling. *Meteo-*
633 *rology and Atmospheric Physics*, **100** (1-4), 3–22.
- 634 Larkin, N. K., and D. Harrison, 2005: On the definition of el niño and associated seasonal average
635 us weather anomalies. *Geophysical Research Letters*, **32** (13).
- 636 Latif, M., and N. S. Keenlyside, 2009: El niño/southern oscillation response to global warming.
637 *Proceedings of the National Academy of Sciences*, **106** (49), 20 578–20 583.
- 638 Leung, L. R., L. O. Mearns, F. Giorgi, and R. L. Wilby, 2003a: Regional climate research: needs
639 and opportunities. *Bulletin of the American Meteorological Society*, **84** (1), 89–95.

- 640 Leung, L. R., and Y. Qian, 2009: Atmospheric rivers induced heavy precipitation and flooding in
641 the western US simulated by the WRF regional climate model. *Geophysical research letters*,
642 **36** (3).
- 643 Leung, L. R., Y. Qian, and X. Bian, 2003b: Hydroclimate of the western United States based on
644 observations and regional climate simulation of 1981-2000. Part I: Seasonal statistics. *Journal*
645 *of Climate*, **16** (12), 1892–1911.
- 646 Maloney, E. D., and Coauthors, 2014: North american climate in cmip5 experiments: part iii:
647 assessment of twenty-first-century projections*. *Journal of Climate*, **27** (6), 2230–2270.
- 648 Maurer, E., A. Wood, J. Adam, D. Lettenmaier, and B. Nijssen, 2002: A long-term hydrologically
649 based dataset of land surface fluxes and states for the conterminous United States*. *Journal of*
650 *climate*, **15** (22), 3237–3251.
- 651 McDonald, A., 2003: Transparent boundary conditions for the shallow-water equations: testing in
652 a nested environment. *Monthly weather review*, **131** (4), 698–705.
- 653 Meehl, G. A., H. Teng, and G. Bannister, 2006: Future changes of el niño in two global coupled
654 climate models. *Climate Dynamics*, **26** (6), 549–566.
- 655 Mesinger, F., and K. Veljovic, 2013: Limited area NWP and regional climate modeling: a test
656 of the relaxation vs Eta lateral boundary conditions. *Meteorology and Atmospheric Physics*,
657 **119** (1-2), 1–16.
- 658 Mesinger, F., and Coauthors, 2006: North American regional reanalysis. *Bulletin of the American*
659 *Meteorological Society*, **87**, 343–360.
- 660 Min, S.-K., X. Zhang, F. W. Zwiers, and G. C. Hegerl, 2011: Human contribution to more-intense
661 precipitation extremes. *Nature*, **470** (7334), 378–381.

- 662 Morrison, H., and A. Gettelman, 2008: A new two-moment bulk stratiform cloud microphysics
663 scheme in the Community Atmosphere Model, version 3 (CAM3). Part I: Description and nu-
664 matical tests. *Journal of Climate*, **21** (15), 3642–3659.
- 665 Neale, R. B., and Coauthors, 2010a: Description of the NCAR community atmosphere model
666 (CAM 5.0). *NCAR Tech. Note NCAR/TN-486+STR*.
- 667 Neale, R. B., and Coauthors, 2010b: Description of the NCAR Community Atmosphere Model
668 (CAM 5.0). NCAR Technical Note NCAR/TN-486+STR, National Center for Atmospheric Re-
669 search, Boulder, Colorado, 268 pp.
- 670 Neelin, J. D., B. Langenbrunner, J. E. Meyerson, A. Hall, and N. Berg, 2013: California winter
671 precipitation change under global warming in the coupled model intercomparison project phase
672 5 ensemble. *Journal of Climate*, **26** (17), 6238–6256.
- 673 Neiman, P. J., F. M. Ralph, G. A. Wick, J. D. Lundquist, and M. D. Dettinger, 2008: Meteorolog-
674 ical characteristics and overland precipitation impacts of atmospheric rivers affecting the west
675 coast of north america based on eight years of ssm/i satellite observations. *Journal of Hydrom-
676 eteorology*, **9** (1), 22–47.
- 677 NOAA, 2013: Defining El Niño and La Niña. Accessed: 2015-
678 08-20, [https://www.climate.gov/news-features/understanding-climate/
679 watching-el-nio-and-la-nia-noaa-adapts-global-warming](https://www.climate.gov/news-features/understanding-climate/watching-el-nio-and-la-nia-noaa-adapts-global-warming).
- 680 O’Gorman, P. A., and T. Schneider, 2009: The physical basis for increases in precipitation ex-
681 tremes in simulations of 21st-century climate change. *Proceedings of the National Academy of
682 Sciences*, **106** (35), 14 773–14 777.

- 683 Oleson, K., and Coauthors, 2010: Technical description of version 4.0 of the Community Land
684 Model (CLM). NCAR Technical Note NCAR/TN-478+STR, National Center for Atmospheric
685 Research, Boulder, Colorado, 257 pp. doi:10.5065/D6FB50WZ.
- 686 Pierce, D. W., 2002: The role of sea surface temperatures in interactions between enso and the
687 north pacific oscillation. *Journal of climate*, **15** (11), 1295–1308.
- 688 Ralph, F. M., P. J. Neiman, and G. A. Wick, 2004: Satellite and caljet aircraft observations of
689 atmospheric rivers over the eastern north pacific ocean during the winter of 1997/98. *Monthly*
690 *Weather Review*, **132** (7), 1721–1745.
- 691 Rauscher, S. A., E. Coppola, C. Piani, and F. Giorgi, 2010: Resolution effects on regional climate
692 model simulations of seasonal precipitation over Europe. *Climate dynamics*, **35** (4), 685–711.
- 693 Rauscher, S. A., T. D. Ringler, W. C. Skamarock, and A. A. Mirin, 2013: Exploring a Global
694 Multiresolution Modeling Approach Using Aquaplanet Simulations. *Journal of Climate*, **26** (8),
695 2432–2452.
- 696 Rhoades, A. M., X. Huang, P. A. Ullrich, and C. M. Zarzycki, 2015: Characterizing Sierra Nevada
697 snowpack using variable-resolution CESM. *Journal of Applied Meteorology and Climatology*,
698 (2015).
- 699 Riahi, K., and Coauthors, 2011: RCP 8.5A scenario of comparatively high greenhouse gas emis-
700 sions. *Climatic Change*, **109** (1-2), 33–57.
- 701 Rowell, D. P., and R. G. Jones, 2006: Causes and uncertainty of future summer drying over europe.
702 *Climate Dynamics*, **27** (2-3), 281–299.

- 703 Salathé Jr, E. P., R. Steed, C. F. Mass, and P. H. Zahn, 2008: A High-Resolution Climate Model
704 for the US Pacific Northwest: Mesoscale Feedbacks and Local Responses to Climate Change*.
705 *Journal of Climate*, **21** (21), 5708–5726.
- 706 Scoccimarro, E., M. Zampieri, A. Bellucci, A. Navarra, and Coauthors, 2013: Heavy precipitation
707 events in a warmer climate: results from CMIP5 models. *Journal of climate*.
- 708 Seneviratne, S. I., and Coauthors, 2012: Changes in climate extremes and their impacts on the
709 natural physical environment. *Managing the risks of extreme events and disasters to advance*
710 *climate change adaptation*, 109–230.
- 711 Sillmann, J., V. Kharin, F. Zwiers, X. Zhang, and D. Bronaugh, 2013: Climate extremes indices
712 in the cmip5 multimodel ensemble: Part 2. future climate projections. *Journal of Geophysical*
713 *Research: Atmospheres*, **118** (6), 2473–2493.
- 714 Simmons, A., K. Willett, P. Jones, P. Thorne, and D. Dee, 2010: Low-frequency variations
715 in surface atmospheric humidity, temperature, and precipitation: Inferences from reanalyses
716 and monthly gridded observational data sets. *Journal of Geophysical Research: Atmospheres*,
717 **115** (D1).
- 718 Singh, D., M. Tsiang, B. Rajaratnam, and N. S. Diffenbaugh, 2013: Precipitation extremes over the
719 continental United States in a transient, high-resolution, ensemble climate model experiment.
720 *Journal of Geophysical Research: Atmospheres*, **118** (13), 7063–7086.
- 721 Small, R. J., and Coauthors, 2014: A new synoptic scale resolving global climate simulation using
722 the community earth system model. *Journal of Advances in Modeling Earth Systems*, **6** (4),
723 1065–1094.

- 724 Staniforth, A. N., and H. L. Mitchell, 1978: A variable-resolution finite-element technique for
725 regional forecasting with the primitive equations. *Monthly Weather Review*, **106** (4), 439–447.
- 726 Stevenson, S., 2012: Significant changes to enso strength and impacts in the twenty-first century:
727 Results from cmip5. *Geophysical Research Letters*, **39** (17).
- 728 Sugi, M., and J. Yoshimura, 2004: A mechanism of tropical precipitation change due to co2
729 increase. *Journal of climate*, **17** (1), 238–243.
- 730 Taschetto, A. S., A. S. Gupta, N. C. Jourdain, A. Santoso, C. C. Ummenhofer, and M. H. England,
731 2014: Cold tongue and warm pool enso events in cmip5: mean state and future projections.
732 *Journal of Climate*, **27** (8), 2861–2885.
- 733 Taylor, M. A., 2011: Conservation of mass and energy for the moist atmospheric primitive equa-
734 tions on unstructured grids. *Numerical Techniques for Global Atmospheric Models*, Springer,
735 357–380.
- 736 Tebaldi, C., K. Hayhoe, J. M. Arblaster, and G. A. Meehl, 2006: Going to the extremes. *Climatic
737 change*, **79** (3-4), 185–211.
- 738 Trenberth, K. E., 2011: Changes in precipitation with climate change. *Climate Research*, **47** (1),
739 123.
- 740 Trenberth, K. E., A. Dai, R. M. Rasmussen, and D. B. Parsons, 2003: The changing character of
741 precipitation. *Bulletin of the American Meteorological Society*, **84** (9), 1205–1217.
- 742 Ullrich, P. A., D. Devendran, and H. Johansen, 2016: Arbitrary-order conservative and consistent
743 remapping and a theory of linear maps, part 2. *Monthly Weather Review*, **144** (4), 1529–1549,
744 doi:10.1175/MWR-D-15-0301.1.

- 745 Ullrich, P. A., and M. A. Taylor, 2015: Arbitrary-Order Conservative and Consistent Remapping
746 and a Theory of Linear Maps: Part I. *Monthly Weather Review*, **143** (6), 2419–2440, doi:10.
747 1175/MWR-D-14-00343.1.
- 748 Walker, M. D., and N. S. Diffenbaugh, 2009: Evaluation of high-resolution simulations of daily-
749 scale temperature and precipitation over the united states. *Climate dynamics*, **33** (7-8), 1131–
750 1147.
- 751 Wehner, M. F., 2013: Very extreme seasonal precipitation in the NARCCAP ensemble: model
752 performance and projections. *Climate Dynamics*, **40** (1-2), 59–80.
- 753 Wehner, M. F., R. L. Smith, G. Bala, and P. Duffy, 2010: The effect of horizontal resolution
754 on simulation of very extreme US precipitation events in a global atmosphere model. *Climate
755 dynamics*, **34** (2-3), 241–247.
- 756 Wehner, M. F., and Coauthors, 2014: The effect of horizontal resolution on simulation qual-
757 ity in the Community Atmospheric Model, CAM5.1. *J. Model. Earth. Sys.*, doi:10.1002/
758 2013MS000276.
- 759 Yoon, J.-H., S. S. Wang, R. R. Gillies, B. Kravitz, L. Hipps, and P. J. Rasch, 2015: Increasing
760 water cycle extremes in california and in relation to enso cycle under global warming. *Nature
761 communications*, **6**.
- 762 Zarzycki, C. M., C. Jablonowski, and M. A. Taylor, 2014: Using Variable-Resolution Meshes
763 to Model Tropical Cyclones in the Community Atmosphere Model. *Monthly Weather Review*,
764 **142** (3), 1221–1239.

- 765 Zarzycki, C. M., C. Jablonowski, D. R. Thatcher, and M. A. Taylor, 2015: Effects of localized grid
766 refinement on the general circulation and climatology in the Community Atmosphere Model.
767 *Journal of Climate*, (2015).
- 768 Zhang, X., L. Alexander, G. C. Hegerl, P. Jones, A. K. Tank, T. C. Peterson, B. Trewin, and
769 F. W. Zwiers, 2011: Indices for monitoring changes in extremes based on daily temperature and
770 precipitation data. *Wiley Interdisciplinary Reviews: Climate Change*, **2** (6), 851–870.
- 771 Zhang, X., J. Wang, F. W. Zwiers, and P. Y. Groisman, 2010: The influence of large-scale climate
772 variability on winter maximum daily precipitation over North America. *Journal of Climate*,
773 **23** (11), 2902–2915.

774 update the mesh grid plot

775 LIST OF TABLES

TABLE 1. Precipitation indices employed in this study.

Name	Definition
Pr	Mean daily precipitation
R1mm	Number of days per year with Pr>1 mm
SDII	Simple precipitation intensity index: Precipitation amount / $\langle R1mm \rangle$ (mm/day)
R5mm	Number of days per year with Pr>1 mm and Pr=<5 mm
R10mm	Number of days per year with Pr>5 mm and Pr=<10 mm
R20mm	Number of days per year with Pr>10 mm and Pr=<20 mm
R40mm	Number of days per year with Pr>20 mm and Pr=<40 mm
Rxmm	Number of days per year with Pr>40 mm
F1mm	Fraction of precipitation contributed to the total precipitation for days of R1mm (similarly for F5mm, F10mm, F20mm, F40mm and Fxmm)
P5mm	Precipitation amount from R5mm (similarly for P10mm, P20mm, F40mm, Pxmm)

777 LIST OF FIGURES

778	Fig. 1. (a) The approximate grid spacing used for the VR-CESM 0.25° mesh. (b) A depiction of 779 the transition from the global 1° resolution mesh through two layers of refinement to 0.25° . 780 (c) Topography height over the study area.	41
781	Fig. 2. Mean precipitation and associated indices from VR-CESM and reference datasets over the 782 historical period, 1980-2005. Areas with statistically significance differences are marked 783 with stippling.	42
784	Fig. 3. Mean precipitation and associated indices from VR-CESM and reference datasets over the 785 historical period, 1980-2005 (continued).	43
786	Fig. 4. Mean precipitation and associated indices from VR-CESM and reference datasets over the 787 historical period, 1980-2005 (continued).	44
788	Fig. 5. The mean precipitation (Pr), 2m average temperature ($Tavg$), and 2m relative humidity (RH) 789 averaged over each time period. Areas with statistically significance differences are marked 790 with stippling.	45
791	Fig. 6. Differences of precipitation indices Pr (mm/day), SDII and $R*mm$ between hist, mid and 792 end average. Areas with statistically significance differences are marked with stippling.	46
793	Fig. 7. Differences of precipitation indices Pr (mm/year) and $P*mm$ between hist, mid and end 794 average. Areas with statistically significance differences are marked with stippling.	47
795	Fig. 8. Changes of specific humidity and horizontal wind pattern at 850hPa for moisture flux il- 796 lustration, and IVT for simulations under different time period of wet season (October to 797 March) averaged over 26 years. (Note: The minimum wind vector is set to be 0.5 m/s, 798 therefore, the wind less than 0.5 m/s is also plotted at the minimum length for better vis- 799 ualization.) Specific humidity and wind pattern are averaged over all days over cool season 800 rather than days with $Pr \geq 10\text{mm}$.	48
801	Fig. 9. Frequency distribution of rainy days ($Pr \geq 0.1\text{mm/day}$) over the three time periods from 802 simulations in four regions (with logarithmic vertical scale). (Note: Region 1 to 4 cover 803 Washington and Oregon; California; Nevada, Utah and Idaho; Arizona and New Mexico, 804 respectively.)	49
805	Fig. 10. Differences of precipitation indices Pr and $R*mm$ between warm and cool phases of ENSO 806 over each time period.	50
807	Fig. 11. Changes of IVT for simulations under different phases of ENSO of wet season (October to 808 March). (Note: The minimum wind vector is set to be 0.5 m/s, therefore, the wind less than 809 0.5 m/s is also plotted at the minimum length for better visualization.)	51

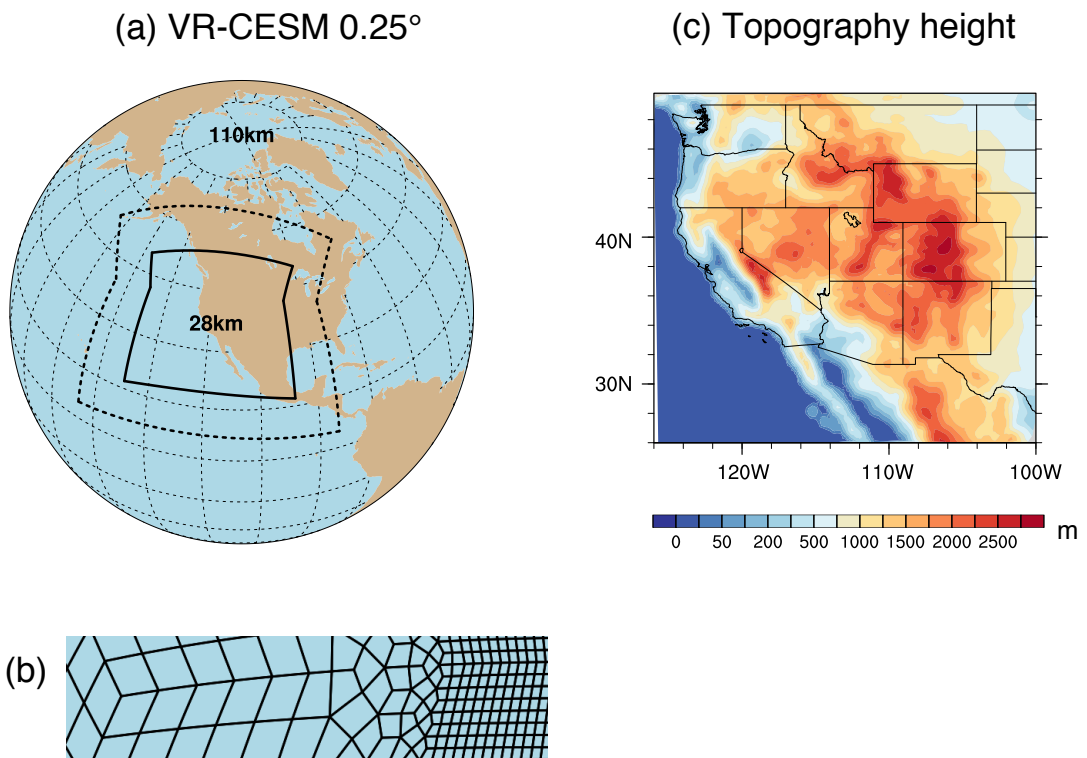
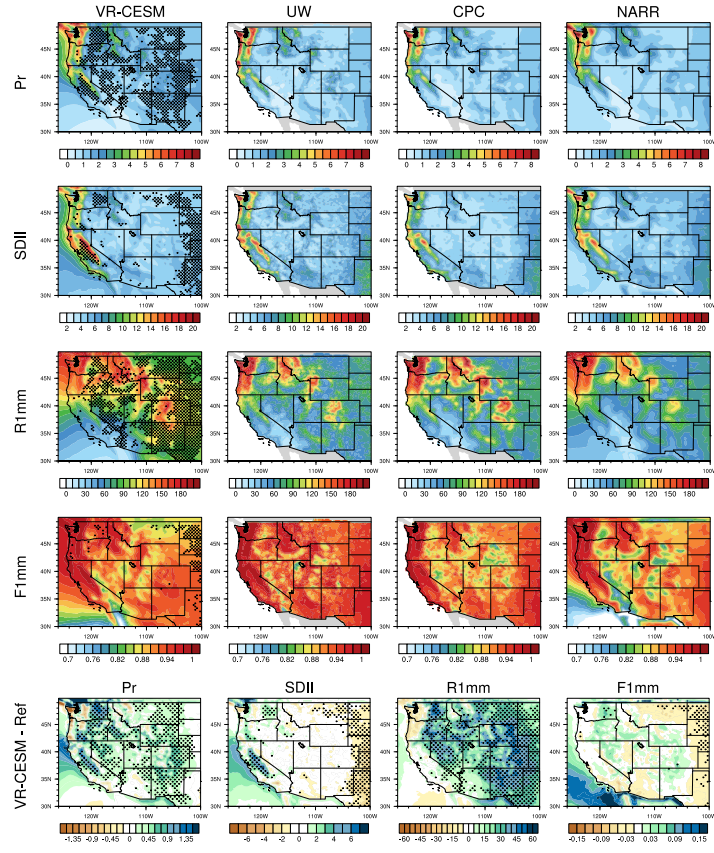
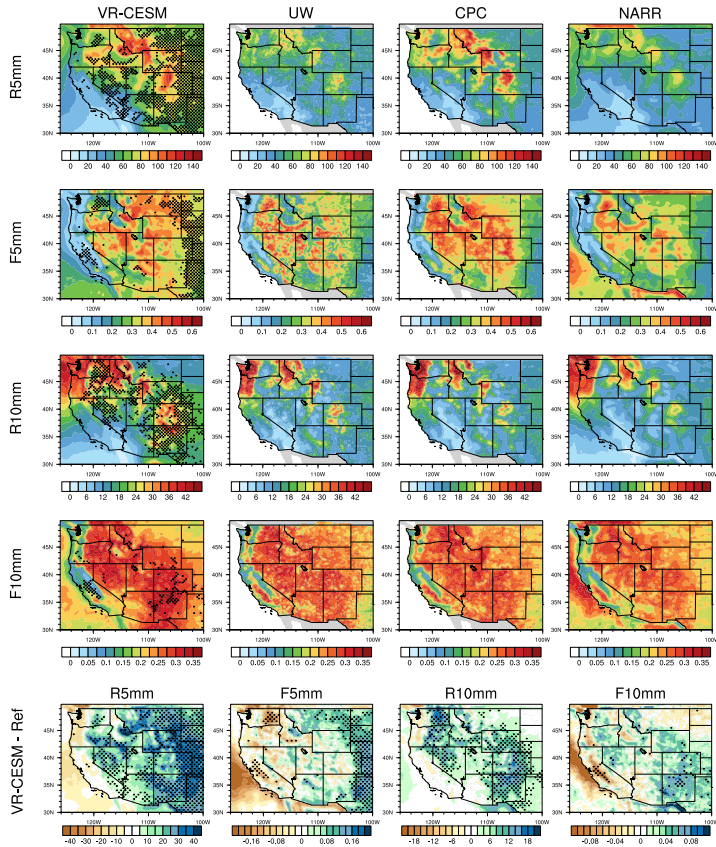


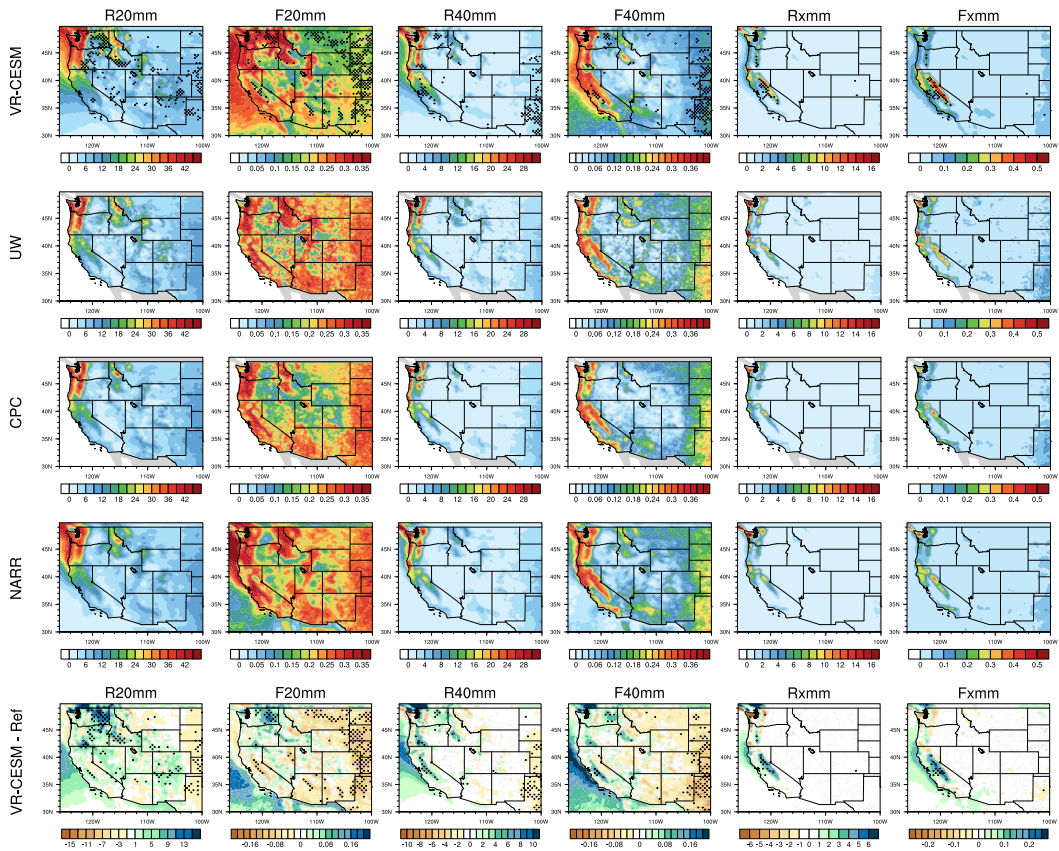
FIG. 1. (a) The approximate grid spacing used for the VR-CESM 0.25° mesh. (b) A depiction of the transition from the global 1° resolution mesh through two layers of refinement to 0.25° . (c) Topography height over the study area.



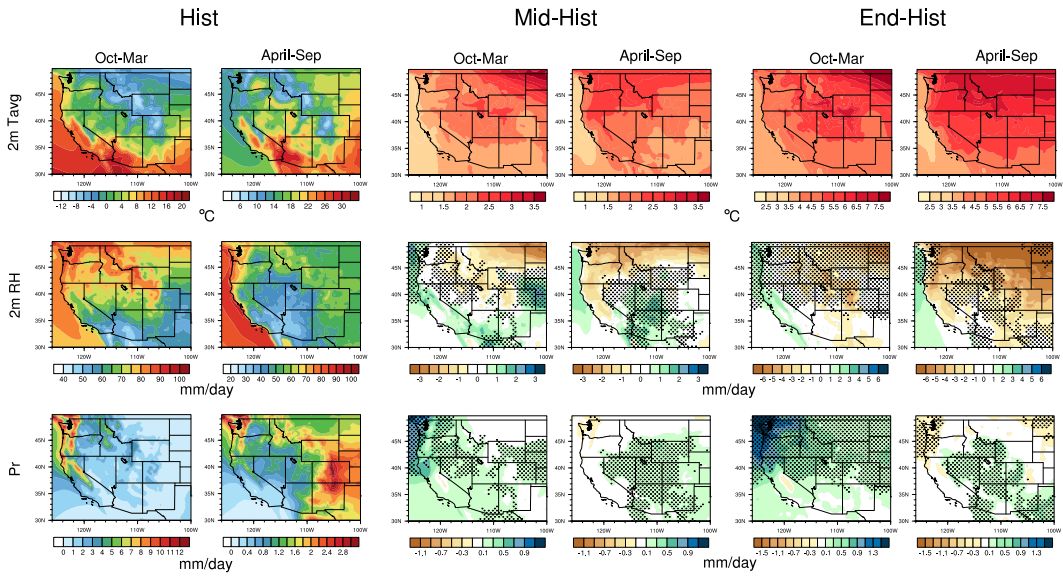
813 FIG. 2. Mean precipitation and associated indices from VR-CESM and reference datasets over the historical
 814 period, 1980-2005. Areas with statistically significant differences are marked with stippling.



815 FIG. 3. Mean precipitation and associated indices from VR-CESM and reference datasets over the historical
 816 period, 1980-2005 (continued).



817 FIG. 4. Mean precipitation and associated indices from VR-CESM and reference datasets over the historical
 818 period, 1980-2005 (continued).



819 FIG. 5. The mean precipitation (Pr), 2m average temperature (Tavg), and 2m relative humidity (RH) averaged
820 over each time period. Areas with statistically significance differences are marked with stippling.

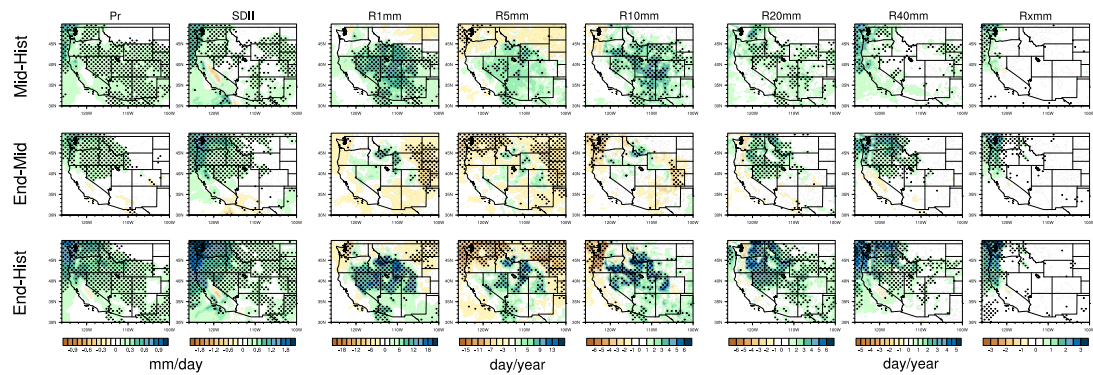
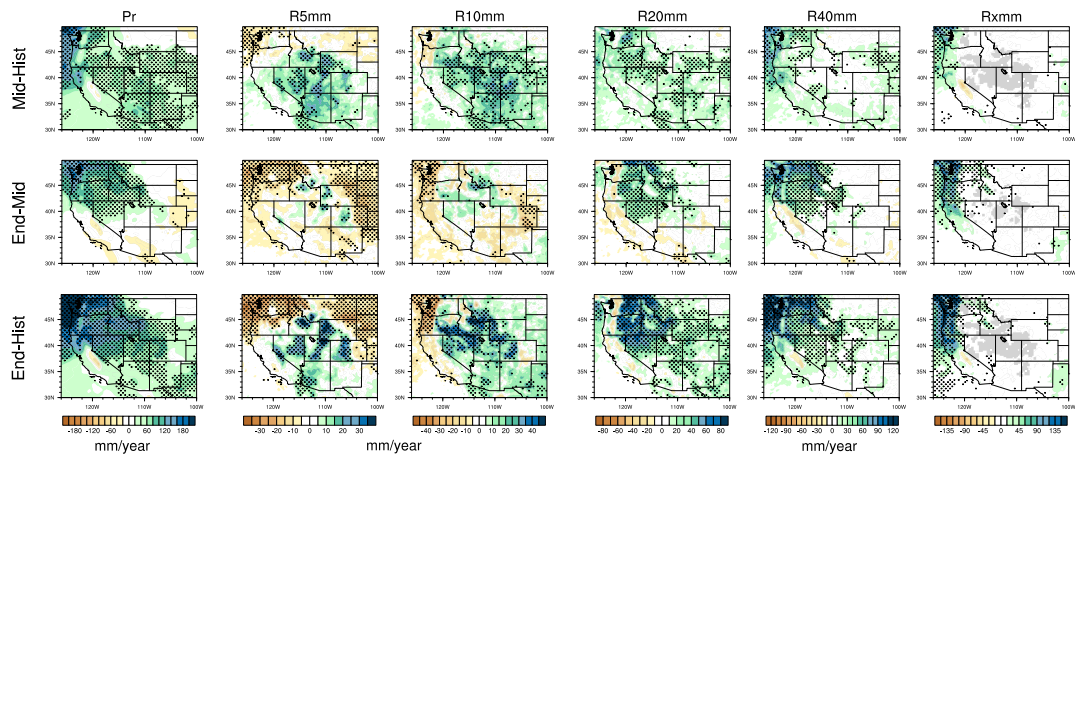
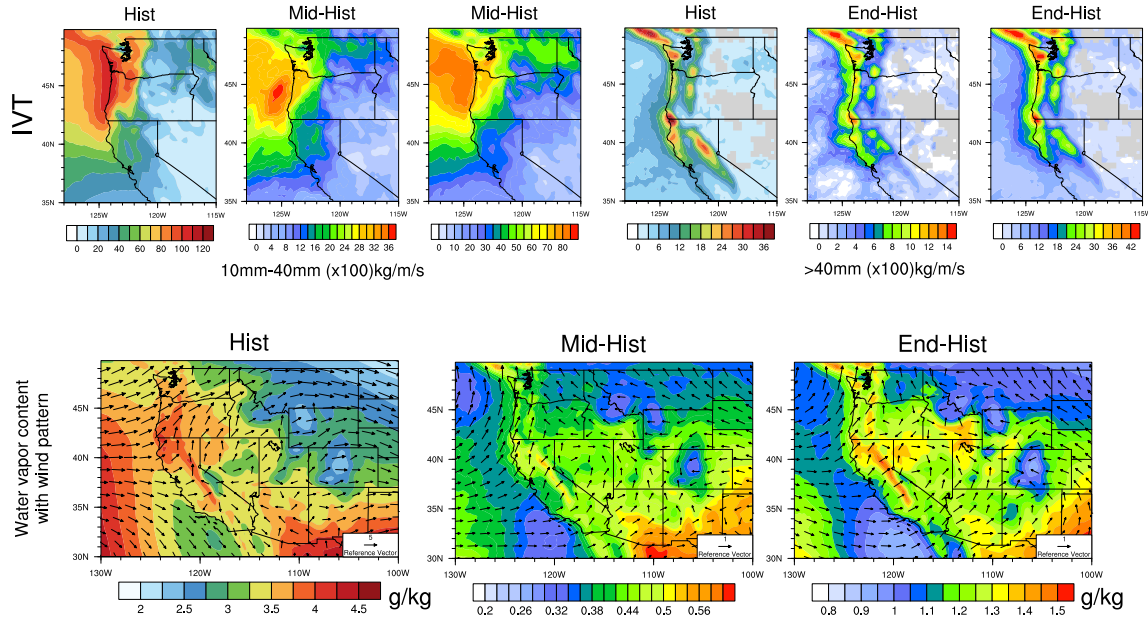


FIG. 6. Differences of precipitation indices Pr (mm/day), SDII and R^* mm between hist, mid and end average.
Areas with statistically significant differences are marked with stippling.



823 FIG. 7. Differences of precipitation indices Pr (mm/year) and $P \cdot mm$ between hist, mid and end average.
 824 Areas with statistically significance differences are marked with stippling.



825 FIG. 8. Changes of specific humidity and horizontal wind pattern at 850hPa for moisture flux illustration,
 826 and IVT for simulations under different time period of wet season (October to March) averaged over 26 years.
 827 (Note: The minimum wind vector is set to be 0.5 m/s, therefore, the wind less than 0.5 m/s is also plotted at the
 828 minimum length for better visualization.) **Specific humidity and wind pattern are averaged over all days over**
 829 **cool season rather than days with $\text{Pr}_t > 10\text{mm}$.**

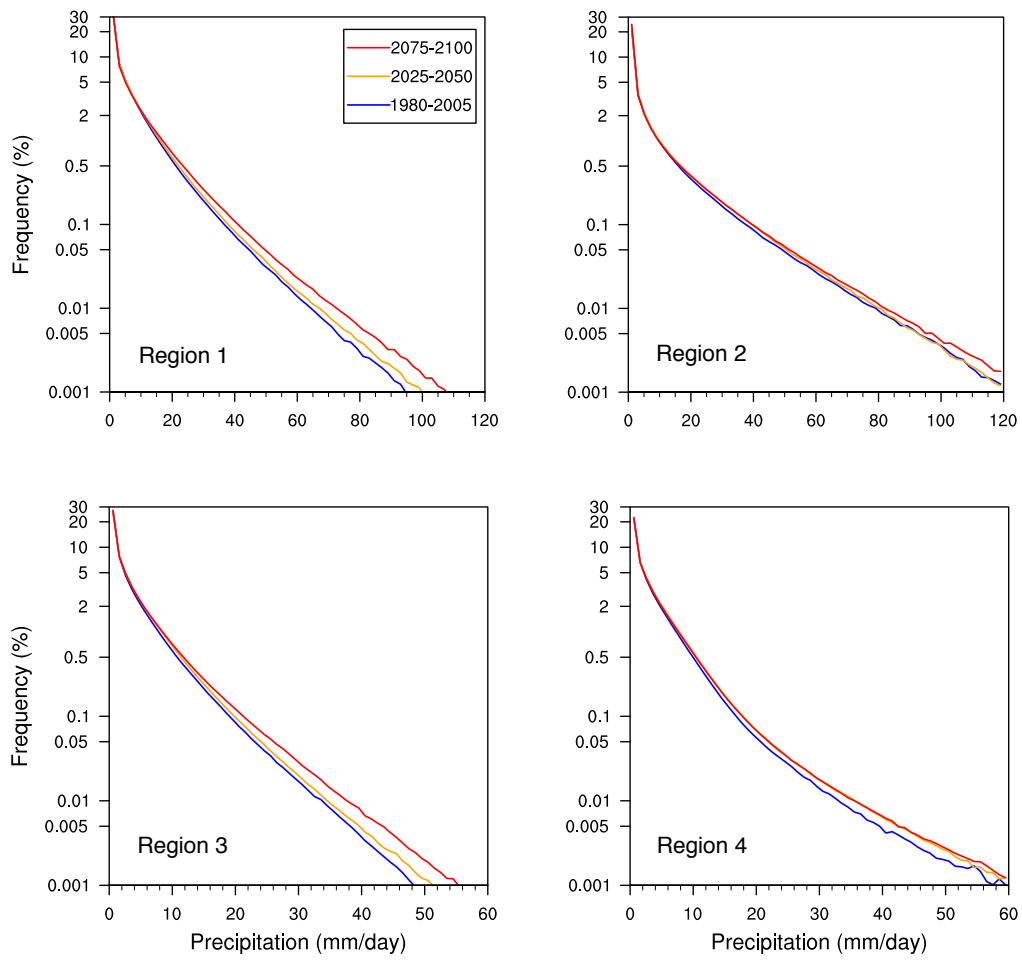
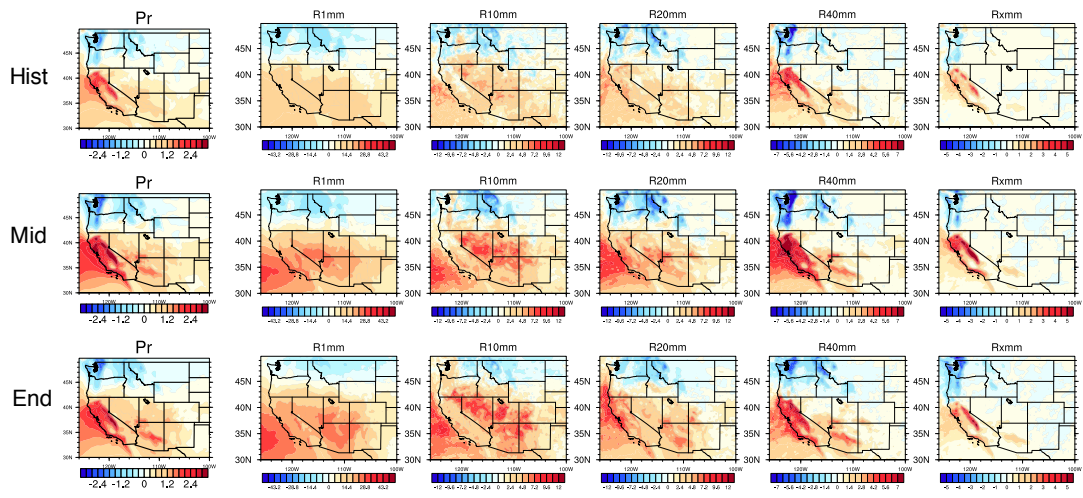
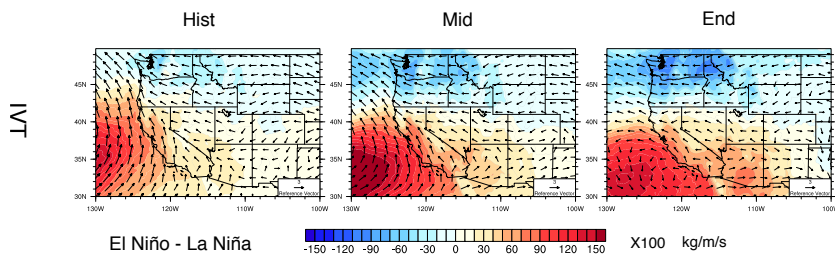


FIG. 9. Frequency distribution of rainy days ($Pr \geq 0.1 \text{ mm/day}$) over the three time periods from simulations in four regions (with logarithmic vertical scale). (Note: Region 1 to 4 cover Washington and Oregon; California; Nevada, Utah and Idaho; Arizona and New Mexico, respectively.)



833 FIG. 10. Differences of precipitation indices Pr and R^*mm between warm and cool phases of ENSO over
834 each time period.



835 FIG. 11. Changes of IVT for simulations under different phases of ENSO of wet season (October to March).
 836 (Note: The minimum wind vector is set to be 0.5 m/s, therefore, the wind less than 0.5 m/s is also plotted at the
 837 minimum length for better visualization.)